Collective pinning model of the mixed state in $YBa_2Cu_3O_{7-\delta}$: Critical currents and flux creep

J. W. Farmer and D. L. Cowan
Research Reactor and Physics Department, University of Missouri, Columbia, Missouri 65211, USA

M. Kornecki*
Weapons & Materials Research, U.S. Army Research Laboratory, Aberdeen Proving Ground, Maryland 21006, USA

(Received 16 February 2007; revised manuscript received 1 June 2007; published 25 February 2008)

Magnetic hysteresis and flux creep measurements in single crystal samples of $YBa_2Cu_3O_{7-\delta}$ (YBCO) are presented for a wide range of B,T phase space. Some of these samples can be described as weakly or collectively pinned. For these, over a large portion of this phase space, the flux creep can be described in terms of thermally activated single-fluxoid motion. A simple model based on maximizing the pinning energy of a fluxoid segment provides a good, semiquantitative picture of the low-temperature data, where the experimentally measured critical current density j is proportional to $1/T$ and the activation barrier height is proportional to $j^{-\mu}$, where $\mu=1$. In this model individual fluxoids are pinned by stochastic fluctuations in defect concentration, and are driven over the pinning barriers by critical currents and thermal activation. Incorporating flux lattice elasticity into this simple model leads to new predictions for the low-temperature data and allows the simple model to be extended to higher temperature. There are two distinct effects, both of which can be put in the form of effective current densities. One effective current density j_s arises from direct fluxoid-fluxoid repulsion, and the second effective current density j_r arises from fluxoid relaxation. In YBCO at 7 K and 2 T, where the measured critical current density is $j=8.9\times10^9$ A/m^2, we find $j_s=0.57\times10^9$ A/m^2 (6%) and $j_r=-2.1\times10^9$ A/m^2 (−20%). We present a discussion of their origin that leads to plausible temperature and field dependences. The model accounts for the rapid drop of $j(T)$ with increasing temperature, the peak effect in $j(B)$ at high temperature, and the temperature and field dependence of the "critical exponent" μ. Thermal fluxoid vibrations play an important role in the pinning, and we find effects consistent with calculations in the literature. The model postulates that fluxoid motion takes place by hopping in segments on a characteristic length scale l_{model}. In the model we find $l_{\text{model}}=104$ nm at 7 K and 2 T. A completely independent measurement from the creep-derived four-volume VX yields a length $l_{VX}=102\pm5$ nm at the same temperature and field. Excellent agreement between the two independently determined lengths persists over a wide range of temperatures. A failure of these two lengths to agree marks the boundary for single-fluxoid hopping, and we present a diagram of the pinning regimes in B,T phase space. From the measured prefactor of thermally activated creep at 10 K and 2 K we infer a value for the attempt frequency $f_a=8.5\times10^{10}$ s^{-1}. This value is in reasonable agreement with a published theoretical calculation of the relaxation frequency for overdamped fluxoids in an Abrikosov lattice. Finally, based on these data we estimate the mass per unit length of a YBCO fluxoid segment, and compare our result with Suhl's theory to obtain a quasiparticle effective mass of 30 free electron masses.

DOI: 10.1103/PhysRevB.77.054514 PACS number(s): 74.25.Qt

I. INTRODUCTION

In 1986, Bednorz and Müller[1] reported the discovery of a transition metal compound with a superconducting transition temperature at 35 K, far above the high-T_c record for the previous 20 years. Soon after, $YBa_2Cu_3O_{7-\delta}$ (YBCO) was discovered to have a T_c above liquid nitrogen.[2] A vast effort has been expended in probing these rich and interesting materials, and there are now hundreds of examples of high-temperature cuprous oxide superconductors. There also is a developing theoretical consensus that these superconductors are examples of doped Mott insulators,[3] with the doping coming either from chemical substitution or by varying the oxygen content. Experimentally, except for the d-wave pairing mechanism[4] (presumably coming from the Cu $3d$ orbitals), the superconducting state itself seems quite conventional. The superconductivity arises from Cooper pairs, and an early study on YBCO observed the hexagonally correlated flux lattice of singly quantized vortices with flux of $\phi_0=h/2e=2.07\times10^{-15}$ T m^2.[5]

Many technological applications depend on the properties of the superconductor in the mixed state. When a current dependent force, usually referred to as a Lorentz force, acts on the fluxoids, these fluxoids must be pinned in place to prevent dissipation. The total energy is reduced when a fluxoid's normal core, of approximate radius ξ, the superconducting order parameter coherence length, overlaps with any defect that suppresses the superconducting order parameter. Extended defects can act as strong pinning centers. These strong pinning defects include twin boundaries, columnar defects produced by heavy ion implantation,[6] fast neutron irradiation defects,[7] and precipitates. Point defects also can act as pinning centers, and it is often suggested that oxygen vacancies are effective point defect pinning centers in these nonstoichiometric systems. Recent scanning tunneling measurements directly confirm the role of oxygen vacancies in pinning.[8] However, in extreme type II materials, point defects are such weak pinning centers that it requires large numbers of them to pin a fluxoid. In this case, it is the sto-

chastic fluctuations in defect concentration that lead to pinning. This type of pinning is often referred to as cooperative or collective pinning.[9] A large body of important results on pinning is presented in two detailed reviews[10,11] However, collective pinning is a complex stochastic problem even for the simple case of single-fluxoid pinning, and there remain substantial disagreements between theory and experiment.

If a sample in the mixed state is perturbed, for example, by a change in the external field, very large currents are induced and fluxoids will flow. The induced currents rapidly fall and very quickly the residual flux motion will be determined by thermal activation. This thermally activated motion is called flux creep and is described by a rate equation for the critical current density j,

$$dj/dt = K \exp[-E_B/kT], \tag{1}$$

where the prefactor K is determined by sample geometry, E_B is the barrier height to thermal activation, and T is temperature.

In an earlier work[12] we adapted a simple collective pinning model for thermally activated motion of single fluxoids. In this model of thermally activated flux creep, the standard picture of stochastic pinning is assumed. Within this picture, consider a segment of fluxoid of length l inside the sample. As this segment moves inward, it encounters a varying pinning potential whose amplitude is of the order $\sqrt{n\xi^2 l}E_1$, where E_1 is the binding energy of a single point defect inside the fluxoid core, n is the pinning defect density, and $\xi^2 l$ is the volume of the fluxoid core. Every time the fluxoid segment moves a distance inward on the order of ξ, it samples a new set of pinning defects, statistically uncorrelated with the previous set. Therefore the rows of potential wells that hold the fluxoid have a depth, or binding energy of $E_B \approx \sqrt{n\xi^2 l}E_1$. This potential energy landscape is sometimes referred to as a washboard potential.[10] In the presence of a current density j the "washboard" becomes tilted and the barrier height to motion of a segment of length l then is given by

$$E_B = \sqrt{n\xi^2 l}E_1 - (j\phi_0 l)\xi, \tag{2}$$

where the second term arises from the Lorentz force induced by the current density.

This local picture of a fluxoid segment leaves about one-half to two-thirds of the full fluxoid length unaccounted for, i.e., the gaps between the wells along the length of the fluxoid where the fluxoid is not pinned. However, as the unpinned segments bulge inward (driven by the Lorentz force), they need only move a very small distance of the order of one or two ξ until they encounter wells of their own to hold them against the external driving force.

In this picture, almost the entire fluxoid is pinned. However, the role of the "kinks" that separate the individually pinned segments must be considered. Elastic stress in these transition sections could easily "unzip" the pinned segments. The kink stress can be relieved by increasing the length of the transition segment, however, unless the length of the transition segment is small compared to the length of the pinned sections, the entire model is irrelevant. Rather surprisingly, both conditions can be met. The extra contribution to the free energy per unit volume of a tilt deformed region[13] is $\delta g = \frac{1}{2}K_T\theta^2$, where K_T is the elastic tilt modulus and θ is the tilt angle. However, in an anisotropic superconductor with weakly coupled planes, the tilt modulus can be dramatically reduced on short length scales.[13–15] For YBCO the reducing factor is $m_1/m_3 \approx 1/25$, where m_1 is the effective mass in the conducting plane and m_3 is the effective mass perpendicular to the conducting plane. Crabtree and Nelson[16] have applied these considerations to a closely related problem and their result gives the energy cost for our transition segment of

$$\partial E \approx \frac{\varepsilon_0}{25}\left(\frac{\xi^2}{d}\right),$$

where

$$\varepsilon_0 = \frac{1}{4\pi\mu_0}\left(\frac{\phi_0}{\lambda}\right)^2$$

is the fluxoid energy per unit length, and d is the transition length and ξ is the transition height. When $\partial E \leq E_1$ a single defect suffices to hold the segment in place. The equality condition is met for a segment of a few nanometers in length. For most experimental conditions the length of the thermally activated pinning segments that move is much greater than this distance.[12] A tentative first approximation is to neglect the elastic energy effects of the kinks in this model.

The essential hypothesis of the simple maximum pinning model (MPM) from Ref. 12 is that drifting fluxoids tend to hang up on obstructions on a length scale with the largest barrier height E_B. Returning to Eq. (2), one can maximize the barrier energy for length by setting $dE_B/dl = 0$ and solving for $l_{\max}$ to obtain

$$l_{\max} = nE_1^2/(2\phi_0 j)^2, \tag{3}$$

and substituting $l_{\max}$ into Eq. (2) gives

$$E_B = n\xi E_1^2/4\phi_0 j. \tag{4}$$

On long length scales the fluxoid is stabilized against the Lorentz force by individually pinned segments of length $l_{\max}$. On short length scales any segments that jump will have a high probability of jumping back. In this picture, there is little or no irreversible motion of the fluxoid except on lengths near $l_{\max}$.

Equations (1), (3), and (4) provide a complete description of the model. There are several reasons to investigate this simple model further. At fixed B and T, we can find the initial barrier height $E_B(j_0)$ from Eq. (1) and the measured initial creep rate value $(dj/dt)_{j_0}$. Combining Eqs. (3) and (4) we find $l_{\max} = E_B(j_0)/\phi_0 \xi j_0$. In Ref. 12, it is found that at $B = 2$ T and $T = 5$ K that $l_{\max} = 75$ nm. This value for the length of fluxoid segment that moves is plausible in magnitude and it is compatible with ignoring the end effects of the kink transition segments. Geshkenbein and Larken[17] show that $E_B \propto T$ except for minor logarithmic corrections. Thus, from Eq. (4), $j \propto 1/E_B \propto 1/T$ and $l_{\max} \propto T^2$. These predictions are confirmed over a limited low temperature range where the material parameters are nearly constant.[12]

Despite these encouraging results, the simple MPM described above has obvious limitations. (1) Experimental data in the literature show that E_B is approximately proportional to $j^{-\mu}$, where the power law coefficient μ is on the order of unity. However, an experimental value of $\mu=1.0$ is never observed over any extended region of B,T phase space, and the departure from unity varies systematically with both temperature and field.[11] (2) A strong field dependence of the current density (a peak effect) is observed in YBCO even at temperatures and fields where single-fluxoid motion is expected.[18] No model consisting of isolated fluxoids driven by a current through a static potential can give a B dependent j at constant T. (3) The simple MPM as presented above is essentially a low-temperature theory. To extend this model to higher temperature, one must include the effects of thermal vibration of the individual fluxoids.[10] In addition, at higher temperature, the role of fluxoid-fluxoid interactions will grow, eventually driving the system to activated flux bundle motion. A higher-temperature model is needed to account for these effects.

In this paper we deal with all of these issues. The experimental details are presented in Sec. II. Results and discussion are given in Secs. III–V. In Sec. III we present an extended maximum pinning model where we postulate that the effects of fluxoid elasticity can be incorporated into the simple MPM of Eq. (2) by adding a phenomenological term ∂j to the critical current density j. Two results immediately follow: (1) The MPM yields a functional form for $E_B(j)$ that is in better agreement with creep data than any power law function, and (2) at low temperature, the MPM predicts a linear temperature dependence for an "effective" power law coefficient $\mu(T)$ in agreement with experiment.[19] We then identify two physical effects that are consistent with the postulated phenomenological term, derive their temperature and/or field dependences, and compare the predictions with data. In Sec. IV we show that in the single-fluxoid hopping regime, the segment length can be measured experimentally independent of any model and show that the experimental data and the MPM predictions are in excellent agreement. We consider this agreement to be by far the strongest support for the MPM. Even the lengths given in Eq. (3) from the simple MPM provide very good agreement for hopping segment lengths at low temperature. The detailed refinements of the MPM given in Sec. III simply extend the excellent agreement between data and model to much higher temperatures. Section V stands nearly independent of any model discussion, but collects some of our results as they apply to the physical nature of the fluxoid. Summary and conclusions are presented in Sec. VI.

II. EXPERIMENT

A. Sample selection

In order to obtain Cooper pairs in a high-T_c superconductor one must add defects or impurities, presumably to break the antiferromagnetism in the Mott insulator. These defects and/or impurities also contribute to the pinning required to sustain large currents. This dual role for the dopants coupled with the difficulty in doping a ceramic material can complicate the problem of sample characterization. In particular, in these ceramic materials the requirement to dope usually implies annealing sequences that may lead to precipitates and defect clusters that act as strong pinning defects. To address this issue, we used two different growth techniques and two different annealing techniques to produce four distinct sets of samples. One growth technique was the self-flux method of Schneemeyer,[20] and the second technique followed the procedure of the Vancouver group, including high temperature soaks.[21] One type of anneal was done for an extended time in flowing O_2 at 450 °C (following Schneemeyer) and the second type of anneal included high-temperature soak stages (following the Vancouver group annealing sequence). These four sets are identified as SS, SV, VS, and VV. The first letter refers to the growth technique and the second letter refers to the type of anneal. Typical sample sizes are $\hat{a}\times\hat{b}\times\hat{c}$ equal to $1\times1\times0.05$ mm^3.

For the purposes of this study, we need to identify samples from this set that contain a minimum of strong pinning defects. The solution of this dilemma is most easily found by inverting the problem. Fast neutron irradiated samples contain many strong pinning defect clusters. (The thermal spike at the end of the primary displacement cascade results in a nearly ideal volume of heavily damaged material, producing a single strong pinning defect.) Thus, fast neutron irradiated samples provide benchmarks of strong pinning against which other samples can be evaluated, as shown in Table I. Here we have characterized each of fourteen distinctly prepared samples, using one semiquantitative measure, and four simple qualitative features that can be readily identified experimentally. In addition to the multiple samples from each of the above four distinct sample sets, the table includes three fast neutron irradiated samples and one untwinned sample obtained from the Vancouver group.[21]

In their classic study of strong pinning, Beasley, Labusch, and Webb[22] show that the barrier is $E_{\text{strong}}\propto(j_{\max}-j)^{3/2}$, where $j_{\max}$ is determined by the strength and number of the strong pinning defects. In general, weak or collective pinning can be approximated by a power law function, $E_{\text{collective}}\propto j^{-\mu}$. In principle, we can distinguish the two types of pinning by comparing creep data fits to the two barrier height functions. Unfortunately, for every initial current density $j_0(T)$, the range of creep data is so limited that the data can be fit to either function. One solution is to fit each set of creep data at fixed T to an amplitude and initial slope, and force both functions to fit that amplitude and slope. It follows that $\mu(j_0)=3j_0/2(j_{\max}-j_0)$. We then fit all samples to the collective pinning expression. For strong pinning samples the inferred value of μ will rise sharply as $j_0(T)$ approaches $j_{\max}$ (as T falls).[23] This sharp rise in μ as temperature falls is a useful criterion for identifying strongly pinned samples. Therefore, in Table I we use $d\mu/dt$, where t is the reduced temperature, as a semiquantitative indication of the nature of the pinning. In addition to this semiquantitative measure, four qualitative features are used in the table: (a) at low temperature $j(T)$ falls rapidly with increasing T (approximately as $1/T$), (b) $j(B)$ develops a broad maximum beginning at about 30 K, (c) $j(B)$ develops a pronounced peak effect beginning at about 50 K, and (d) in the range of 5–40 K, $\mu(T)$ initially rises and then falls.

TABLE I. Sample characterization. The number preceding the set name is the number of samples in the set. $d\mu/dt$ is the average value for the set. Columns (a)–(d) refer to the four features characteristic of weak pinning. A one indicates it is observed and a zero indicates it is not observed. The set naming convention and the characteristics are given in the text. Data for both VS samples are included to emphasize the correlation between pinning character and $d\mu/dt$.

Type of pinning	Sample set	$d\mu/dt$ 5–10 K	(a) $j \propto 1/T$ 5–20 K	(b) $j(B)$ broad max 30–40 K	(c) $j(B)$ peak 50–80 K	(d) $\mu(T)$ max ≈20 K
Weak	(3) SS	1.7	1	1	1	1
Incipient strong	(3) SV	−3.2	0	1	1	0
Mixed	(2) VS	−2.6	0	1	0	0
		−5.0	0	0	0	0
Strong	(2) VV	−8.2	0	0	0	0
Strong	(3) Irradiated	−9.5	0	0	0	0
Strong	(1) Untwinned	−13.0	0	0	0	0

We note that all three of the fast neutron irradiated samples exhibit large, negative values for $d\mu/dt$, as expected for samples dominated by strong pinning defects. None of the fast neutron irradiated samples display any of the four qualitative features listed above. In contrast, all of the SS samples have a *positive* $d\mu/dt$ (as will be shown in Sec. III, a positive value is expected for collective pinning) and they all display each of the four features in Table I. We therefore attribute the four features above as indications of collective pinning. It is of particular note that the untwinned sample displays a very clear indication of strong pinning, even though there are no twin plane boundaries in this sample. Presumably precipitates are the source of strong pinning defects in this sample. This finding also supports an argument that even though twin boundaries may act as strong pinning sites, they do not play a dominant role in pinning when the spacing between twins is large compared to the flux lattice spacing. For the phase space investigated in the paper, this condition is met in our twinned samples with the possible exception of the high temperature and low field regime where the twin boundaries may suppress a tendency for fluxoid entanglement.[13]

Nowhere in this discussion do we mean to suggest that it is difficult to prepare samples dominated by collective pinning. The four features we use as criteria for collective pinning are widely reported in the literature.[10,11] Specific examples include but are not limited to: item (c) Abulafia[24] (note, they report only data at higher temperature, however, as discussed later, high temperature data in our samples replicate their results) and Kupfer[18] (in heavily doped samples) and item (d) reported by Thompson *et al.*[19] Based on this characterization, we conclude that pinning in our "SS" samples is dominated by the collective or cooperative pinning of weak pinning defects. The other three sets of samples fall into categories with various degrees of strong pinning influence. All of our SS samples are similar and have current densities near 1 MA/cm^2 at low temperature. Based on our semiquantitative measure $d\mu/dt$, one SS sample has the least influence from residual strong pinning defects. In this paper we use the above four features and data from our "best" sample to modify and test the theory. However, our results remain essentially unchanged for data from any of our SS samples.

B. Measurements

Flux creep and hysteresis data were obtained using a Quantum Design SQUID magnetometer. Critical currents were obtained from magnetic moment measurements assuming the Bean critical state.[25] Care was taken to compare our magnetometer results with micro-Hall probe measurements by Abulafia *et al.*[24,26] We find excellent quantitative agreement with the micro-Hall data for both hysteresis and creep data indicating that the volume averaging effect of the magnetometer does not introduce any significant distortion of our results.

In creep measurements we find that the decay of the magnetic moment with time is well fit to the analytic function $m(t)=m(t_0)+A\ \ln[1+(t-t_0)/\tau]+B\ \ln^2[1+(t-t_0)/\tau]$, where t_0 is the time of the initial measurement and A, B, and τ are fitting parameters. This three-parameter fit provides excellent agreement with relaxation data.[12] The instantaneous magnetic moment and its time derivatives used in this study were obtained using this analytical formula. In addition, "creep in" and "creep out" experiments were averaged to eliminate a small correction factor associated with the fact that the creep rate is different depending on whether the sample is in the critical state for increasing or decreasing fields.[22]

The barrier height at initial time t_0 (approximately 60 s for our measurements) was determined using a global graphical technique.[27] Our results, in agreement with Maley *et al.*[27] and others,[11] confirm that the initial barrier height is proportional to temperature as determined from the classic solution to the rate equation.[17] For the sample used in this study we obtained $E_B(j_0)=(23.0\pm0.5)kT$.

Critical currents were obtained from the magnetic moments under conditions of full flux penetration, i.e., for samples in the Bean critical state. Failing to reach full flux

penetration leads to anomalously fast creep. The requirement for full flux penetration prevents meaningful creep measurements at small fields and low temperature, where the currents are large. At the same time, the production of a Bean critical state for the "creep out" mode requires very large fields when j is large, again limiting our range at low temperature. It is not sufficient to simply reach the Bean critical state. In order to avoid significant variation in the field across the sample, one must apply fields well above the Bean critical field. This additional constraint is not always well met at temperatures of 30 K and below.

III. PINNING—RESULTS AND DISCUSSION

A. Pinning models

1. Standard model

The standard model of collective pinning of single fluxoids is discussed in detail in the review by Blatter *et al.*[10] In their review they address the apparent paradox that a pinning force that arises from stochastic fluctuations must grow as the square root of length and thus cannot pin a long stiff fluxoid against any finite current density. They note that when a fluxoid is allowed to relax, it introduces an elastic strain. They then obtain a critical pinning length L_c by minimizing the free energy per unit length when this strain energy is included. In this relaxed state, segments of length L_c are pinned independently and balance the Lorentz force to determine a critical current density j_c, hence resolving the apparent paradox.

Further results based on the standard model provide a derivation of the binding energy $E_B(j)=E_c(j_c/j)^{\mu}$, where E_c is a constant determined by material parameters of the superconductor, including the average density of weak pinning centers, and j_c is the depinning current density. The power law coefficient μ is obtained from scaling arguments[28] and the authors find that $\mu=1/7$ and by inference that $j\propto 1/T^7$. Neither result has been substantiated by experiment. In this paper, we present an alternative model for the collective pinning of single fluxoids.

2. Maximum pinning model

We present an alternative model that is based on an extension of the simple model discussed in the Introduction. In the following section we supplement Eq. (2) with two additional contributions to the barrier height seen by a moving segment. These effects involve, respectively, local elastic strain and the dynamics of motion. Each contributes a term that is proportional to length. The constant of proportionality of each of these terms has units of energy per unit length and can be written as $(\partial j)\phi_0\xi$, where ∂j is an effective current density. Note that this effective current density is artificial; however, it provides a simple mathematical solution to the expanded equation. The measured critical current density j in Eq. (2) is simply replaced with $j+\partial j$. As before, setting $dE_B/dl=0$ and solving for $l_{\max}$ leads to

$$l_{\max}=\frac{nE_1^2}{4\phi_0^2(j+\partial j)^2}, \tag{5}$$

and

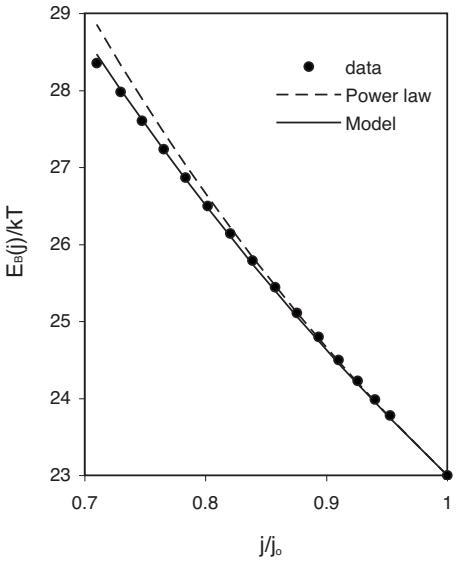

FIG. 1. $E_B(j)$ is obtained from creep data measurements at 2 T and 50 K. The solid circles are the data, the dashed line is the power law model, and the solid line is the single-fluxoid collective pinning model.

$$E_B=\frac{n\xi E_1^2}{4\phi_0(j+\partial j)}. \tag{6}$$

Since this form for the barrier height is no longer a power law function of j, the MPM now predicts that creep data should deviate from the power law form given by scaling arguments. Creep data at 2 T and 50 K are shown in Fig. 1. The solid line is the fit based on the MPM [Eq. (6)], and the dashed curve is a power law curve that has the same magnitude and initial slope as the data. Both functions fit the data reasonably well, especially in the early creep data. However, as j falls, the power law function rises too steeply and begins to systematically deviate from the data. Both curves are one parameter fits where $\mu(j_0)$=constant is the fitting parameter for the power law function at the start of the creep and $\partial j/j_0$=constant is the fitting parameter for the MPM where j_0 is the initial critical current measurement of the creep experiment. In this example $\mu(j_0)=0.64$ and $\delta j/j_0=0.56$. For comparison, at 2 T and 20 K the corresponding values are $\mu(j_0)=1.42$ and $\partial j/j_0=-0.30$. In this case (data not shown), the power law function rises too slowly while the maximum pinning model continues to give very good agreement with the data. In all cases the MPM provides significantly better agreement with the data than the power law model (except when $\mu\approx 1$, where the two models are indistinguishable). No plausible j dependence in the prefactor K from Eq. (1) would alter these conclusions.

As discussed earlier, much of the creep data for high-T_c superconductivity has been interpreted in terms of a power law expression that can be written as $E_B(j)=E_0(j_0/j)^{\mu}$, where E_0 is the barrier height at the start of the creep. From Eq. (6) we can write $E_B(j)=E_0(j_0+\delta j)/(j+\delta j)$. We note that by setting

$$\mu(j_0) = \frac{j_0}{j_0 + \partial j}, \tag{7}$$

these two expressions for $E_B(j)$ will have the same magnitude and initial slope versus current density. As shown in Fig. 1 for all but the most precise measurements, these two expressions for the barrier height remain nearly identical as j falls during the creep process. We can use this near identity to facilitate comparison between results of the MPM and those in the literature that are interpreted in terms of a power law function.

At sufficiently low temperature there will be negligible temperature dependence in any of the material parameters. However, j_0 depends on temperature and using $E_B(j_0) = 23kT$, Eq. (6), and Eq. (7) one can show exactly that

$$\mu(j_0, T) = 1 + cT, \tag{8}$$

where c is a constant. The prediction of the temperature dependence for $\mu(j_0, T)$ given by Eq. (8) is in excellent agreement with low temperature data (see Thompson *et al.*[19] and data shown in Fig. 2 in Sec. III D).

Both the creep data and the observed temperature dependence of "μ" lend strong support to the argument that elasticity effects can be modeled by incorporating an effective current density ∂j into the expression for the barrier height in Eq. (2). In the next section, we discuss possible sources for this new term.

B. Effective current density ∂j

We identify two physically plausible effects that can contribute to the barrier height for single-fluxoid motion. One effect arises from the repulsive force between neighboring fluxoids.[29] This force is responsible for ordering of the flux lattice at low temperature, as directly observed in YBCO.[5] The fluxoid-fluxoid interaction also determines the elastic constants of the flux lattice. The effect of this force on flux creep can be estimated by considering a long fluxoid of length L. In our view, during creep the moving fluxoid exhibits a walking motion. A segment that is activated will leap a distance of a few ξ ahead of its adjacent neighbors, and remain there until the adjacent segments later move ahead. It will always be the lagging segments that jump. Presuming a segment of length l lags a distance ξ, elastic forces lower the binding energy of this segment by an amount of order

$$\partial E_s \approx \frac{\mu_e}{2}\left(\frac{\xi}{a_0}\right)^2 (a_0^2 l),$$

where the local strain is approximately ξ/a_0, the appropriate volume is $a_0^2 l$, a_0 is the average flux lattice spacing, and μ_e is an elastic modulus. It is likely that no single elastic modulus will be appropriate over the entire B,T phase space. However, de Gennes and Matricon[29] observe that for most effects, the elastic tensor can be replaced with a single modulus. Since our interest is in a flowing stream of fluxoids, the appropriate single modulus must be the shear modulus

$$\mu_{\text{shear}} = \left(\frac{4\pi}{\mu_0}\right)\frac{\phi_0 B}{64\pi^2\lambda^2},$$

where μ_0 is the permeability constant, B is the applied field and λ is the magnetic screening length. This shear energy term can be written as an effective current density

$$j_s = \frac{\beta\mu_{\text{shear}}\xi}{2\phi_0}, \tag{9}$$

where β is a dimensionless adjustable constant on the order of unity that can be obtained from fitting to the data.

There is a second physical effect that can alter our basic equation for the barrier height and it also yields an effective current density term. The origin of this term is the relaxation of the fluxoid segment configuration that occurs very shortly after it is trapped. Poole, Farach, and Creswick[30] point out that a moving fluxoid responds to the underlying defect potential energy landscape fairly well. However, immediately after a segment is trapped it will take some time to optimally conform to the local landscape—both because of thermal excitations from its motion and because of the many constraints in reorganizing on a fine scale. The final stage of conformation presumably will involve deformations of amplitude of order ξ (determined by the superconducting order parameter) that add at most a few net defects to the pinning (the moving fluxoid likely will respond to distortions that add more defects). When a moving fluxoid fails to respond on this level, the additional pinning energy gain from a distortion of a trapped fluxoid segment will appear as a kind of static friction. We define a characteristic length l_c along the segment that equates the strain energy of the distortion with the binding energy of a single defect. Distortions shorter than this length cannot produce a net gain in fluxoid binding. This characteristic length is $l_c \approx \varepsilon_0\xi^2/E_1$. The net pinning energy gain of a trapped fluxoid segment that fully conforms to the local environment will then be

$$\partial E_r \approx \alpha E_1 \frac{l}{l_c} \approx \alpha\frac{E_1^2}{\varepsilon_0\xi^2} l,$$

where α is the effective number of additional pinning defects gained from a distortion of length l_c and l/l_c is the average number of distortions in length l. While this derivation is little more than a simple dimensional analysis, it allows us to obtain an estimate for this energy term that can be used in the model. This pinning energy contribution also can be written as an effective current density

$$j_r = -\frac{\alpha E_1^2}{\phi_0\varepsilon_0\xi^3}. \tag{10}$$

The negative sign indicates that this effective current density increases the barrier height. We assume that $\alpha \approx 1$. If α is much larger, such configurations would likely be picked up by moving segments and hence, would not contribute to the additional "static binding." In any case, we can treat α as an adjustable, dimensionless parameter to be determined from the data.

The net effective current density ∂j is the sum of these two terms [Eqs. (9) and (10)]. We obtain the temperature and/or field dependences of these terms in the next section.

C. Temperature and field effects

Implicit temperature dependence is introduced in part through the two material parameters that characterize the superconductor, $\lambda(t)$ and $\xi(t)$, where t is the reduced temperature. Since most of our data are in phase space far from the Ginzburg-Landau (GL) limit, we use the experimentally measured temperature dependence $\lambda(t)^2=\lambda_0^2/(1-t^4)$,[31] with $\lambda_0=140$ nm. The experimental measurements of $\lambda(t)$ are consistent with the standard two-fluid model, therefore we also assume $\xi(t)^2=\xi_0^2(1+t^2)/(1-t^2)$ with $\xi_0=1.4$ nm [although the results remain essentially unchanged if the GL temperature dependence is used for $\xi(t)$]. The remaining temperature dependent terms are $\varepsilon_0(t)\propto 1/\lambda(t)^2$, $E_1(t)\propto \xi^3 H_c^2 \propto \xi(t)/\lambda(t)^2$, where $H_c$is the thermodynamic critical field, and $\mu_{\text{shear}}\propto(\xi(t)/\lambda(t))^2$. The shear modulus also is proportional to B. The low temperature value for the product nE_1^2 is measured from experiment. If the pinning defect concentration n is given by the oxygen vacancy concentration, then for our sample $n\approx 9\times 10^{26}$ m^{-3} and $E_1(0)\approx 3\times 10^{-22}$ J≈ 2 meV.

Thermal fluctuations of the flux lattice are known to reduce the effectiveness of collective pinning. Many authors discuss flux lattice fluctuations.[10,13–15,32] Here we follow the notation of Fisher, Fisher, and Huse[15] for anisotropic material. For YBCO, the mean-square-vortex line displacement W is given by

$$W=\langle (x-x_0)^2\rangle = 5\pi\mu_0\sqrt{\phi_0/B}\lambda^2 kT/\phi_0^2. \tag{11}$$

For large amplitudes of fluctuations it has been argued that the pinning effectiveness is reduced in proportion to $1/W$.[10] The exact functional dependence of the reduction in pinning is not known. In order to have a rough guide to temperature dependence, we assume that the E_1^2 terms in the MPM should be replaced with $f(W)E_1^2$ where $f(W)=1/[1+(W/\xi^2)^2]$. This assumed form of $f(W)$ has the correct physical limits for both large and small W.

D. Effective $\mu(B,T)$ and critical current density $j(B,T)$

Using the above temperature and field dependences, $E_B(j_0)=23$ kT, and Eqs. (6) and (7), it can be shown that the explicit form for $\mu(B,T)$ is

$$\mu(B,T)=1+\alpha\frac{92kT_c(4\pi\mu_0)\lambda_0^2}{n\phi_0^2\xi_0^4}\frac{t}{(1+t^2)^2}\frac{1-t^2}{1+t^2} - \beta\frac{92kT_c\phi_0 B}{8(4\pi\mu_0)\lambda_0^2 nE_1(0)^2}\frac{t}{(1+t^2)^2}\frac{1}{f(W)}, \tag{12}$$

where $T_c=91$ K in our overdoped sample. Note that at low temperature, Eq. (12) reduces to the same low-temperature form given in Eq. (8). All terms in this expression are known or can be measured independently except for the two adjustable parameters α and β. It also follows that the critical current density is given by

$$j(B,T)=\frac{\xi_0 nE_1(0)^2}{92kT_c\phi_0}\left(\frac{1+t^2}{1-t^2}\right)^{3/2}\frac{(1-t^4)^2}{t}f(W)\mu(B,T). \tag{13}$$

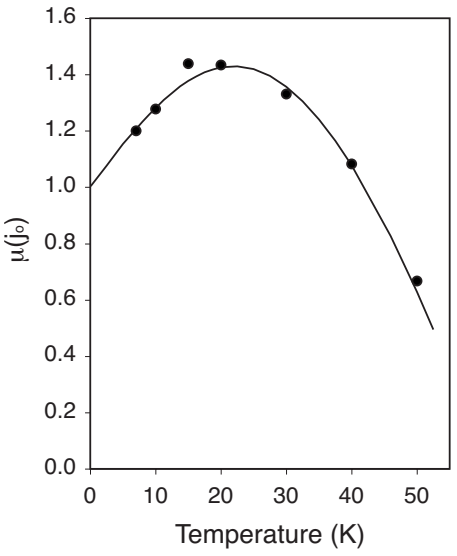

FIG. 2. The dynamic model is compared with $\mu(T)$ data. The solid circles are the data and the solid line is the model prediction.

The adjustable parameters can be fixed by measuring $\mu(B,T)$ at 2 T and at two different temperatures. Choosing 7 K and 40 K as measurement points, and solving for the two unknowns gives $\alpha=1.5$ and $\beta=0.49$ in satisfactory agreement with our earlier discussion. From Eqs. (9) and (10) these parameters give the low-temperature values for the effective currents as $j_r=-2.1\times 10^9$ A/m^2 and $j_s=(B/\text{T})0.28\times 10^9$ A/m^2. As seen in Fig. 2, the agreement between the MPM prediction for $\mu(B,T)$ [Eq. (12)] and experimental data is excellent. The data are for $B=2$T. In particular, the initial rise, the extremum, and the fall of the effective coefficient $\mu(B,T)$ are all described very well.

The prediction for $j(B,T)$ in Eq. (13) is readily evaluated using hysteresis data. At 2 T, Eq. (13) describes the rapid fall in critical current density at low temperature and continues to provide excellent agreement with experiment up to and including 50 K. A more stringent test of the MPM prediction for $j(B,T)$ is found in the data for the field dependence of the critical current density at constant temperature. In samples not dominated by strong pinning defects, a peak effect is clearly seen in experimental data at 30 K (see Table I). Data from our SS sample are compared with Eq. (13) in Fig. 3. The qualitative features of the peak effect are modeled fairly well. However, in detail the model consistently predicts too strong a rise in $j(B)$ at low field and the model does not fully capture the experimentally observed shift in peak field with temperature. These shortcomings are not surprising given the

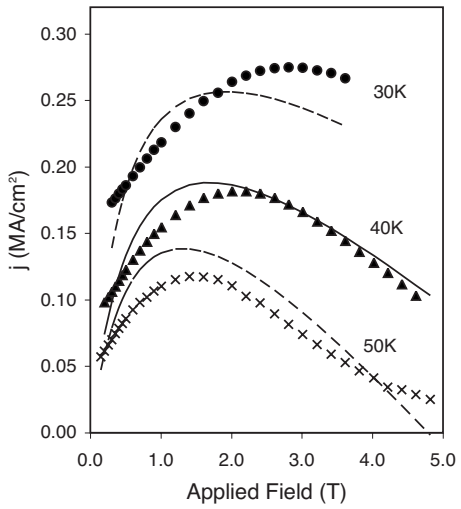

FIG. 3. The MPM model is compared with hysteresis data at various temperatures. The solid circles are the 30 K data, the solid triangles are the 40 K data, and the x's are the 50 K data. The model results are a dashed line, solid line, and dot-dashed line, respectively. For reference, note that the nearly B independent j_c at 5 K and 2 T is 1.1 MA/cm^2, or about 3.4 times the full scale of the graph.

severe restrictions on the parameters used to evaluate the model. In particular, one parameter ξ is used to represent four distinct parameters in this complicated stochastic problem: the coherence length of the order parameter, the flux core radius, the distance to the barrier height, and the strain length that leads to the shear stress. Each of these parameters may have different field and temperature dependences. While recent measurements[33] provide some data for the field and temperature dependence of the flux core diameter, little or no data are available for the other two parameters. In addition, while our data are quantitatively similar to micro-Hall measurements, there remain issues associated with nonuniform internal fields (especially at lower temperatures) and corner effects associated with the rectangular geometry of the sample. It is not the aim of this paper to provide a semiempirical best fit to all of the experimental data, but rather to show that by using reasonable assumptions for the various parameters, the MPM can be used to describe a wide variety of experimental results. In this regard, the model is quite successful. It provides excellent quantitative agreement with three of the four criteria for collective pinning described in Sec. II and qualitative agreement with the fourth, the peak effect.

The MPM for single-fluxoid hopping also makes a clear prediction for the field dependence of μ. The low field value is always greater than one. As the applied field is increased, μ will gradually fall. At fields above the peak, μ will fall rapidly. Unfortunately, the high critical current density in our samples prevents the setting up of a Bean critical state at low magnetic fields. By the time one reaches a temperature with sufficiently low critical current everywhere, the flux transport is beginning to transition into the small bundle regime (see the following section). This restriction frustrates a quantitative comparison, but there is qualitative agreement when the sample is just on the verge of being "single fluxoid," i.e., our field dependent measurements at 68 K and 70 K (similar to Abulafia[24]) clearly show the rapid fall of μ with increasing field above the peak.

IV. LENGTH SCALES AND PHASE BOUNDARIES—RESULTS AND DISCUSSION

Consider a coherent volume of magnetic flux that moves by thermal activation over a landscape of potential barriers. In the presence of a current, the pinning force density must balance the Lorentz force density, $F_V = j \times B$. It then follows that the change in barrier height with current is given by

$$dE_B/dj = BVX, \tag{14}$$

where V is the coherent volume of the flux bundle undergoing thermal activation and X is the distance needed to translate the bundle to the barrier maximum. By expanding Eq. (1) about j_0 it can be shown that

$$VX = (kT/B)\left(\frac{d^2j}{dt^2}\right) \Big/ \left(\frac{dj}{dt}\right)^2. \tag{15}$$

Beasley and Webb[22] were the first to point out that the physically meaningful product VX (sometimes called the "four volume") can be obtained directly from creep measurements.

For the purposes of testing model predictions, it is useful to define a length (which may or may not be physically meaningful) associated with the four volume as

$$l_{\text{Webb}}(B,T) \equiv VX/a_0^2\xi. \tag{16}$$

The MPM also has a characteristic length. From Eqs. (5) and (6),

$$l_{\text{model}}(B,T) = \frac{4(23kT_c)^2}{\xi_0^2 nE_1(0)^2}\frac{t^2(1+t^2)^4}{f(W)}. \tag{17}$$

Note that Eq. (17) gives the same low-temperature prediction as the simple maximum pinning model, i.e., $l \propto T^2$. If the system actually consists of single fluxoids with $X=\xi$, then Eq. (16) should represent the length of the hopping-fluxoid segment. It then follows that if the two lengths are the same, one has strong support for the MPM of single-fluxoid flux creep. The two lengths are shown in Fig. 4 for applied fields of 2 T. For the MPM calculation [Eq. (17)], the measured low-temperature current density is used to evaluate $nE_1(0)^2$. The two lengths agree remarkably well as a function of temperature up to and including 50 K. In addition, the predicted T^2 dependence is observed at low temperature, however, small deviations from an exact T^2 dependence due to the temperature dependence of the material parameters can be seen even at 20 K (data not shown).

The agreement between the two lengths is strong evidence in support of single-fluxoid motion in this region of phase space and provides a very strong confirmation of the predictions of the MPM. We note that at 60 K, the two lengths differ by almost a factor of two. Data at higher temperatures at various fields are included in the inset of Fig. 4. For the higher-temperature data the difference between the two lengths is approximately a factor of 3. The region where the

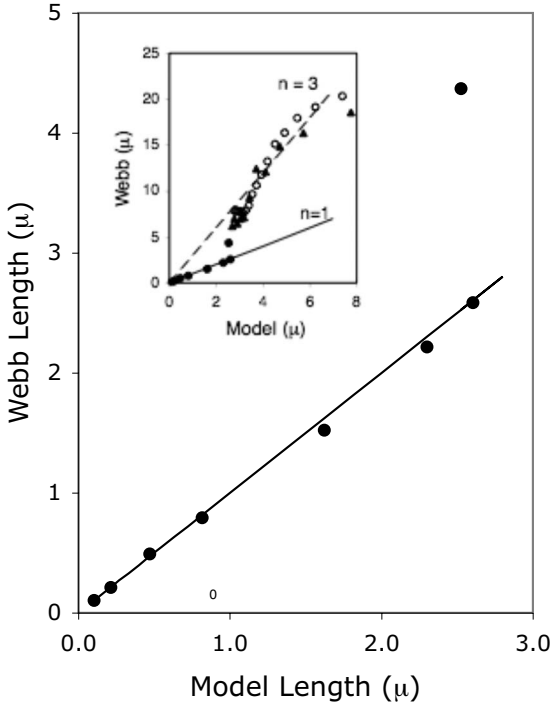

FIG. 4. The experimentally measured four volume yields a characteristic "Webb" length that is plotted vs the predicted characteristic length given by the maximum pinning model. The solid circles are the results at the 2 T field for temperatures from 7 to 60 K. All data except for the 60 K point fall near the solid line that has a slope of one. Results at 68 and 70 K vs field are shown in the inset. Low field data start at the upper right and systematically track down and to the left as the field is increased. The high-temperature data vs field lie near the solid line with a slope of three.

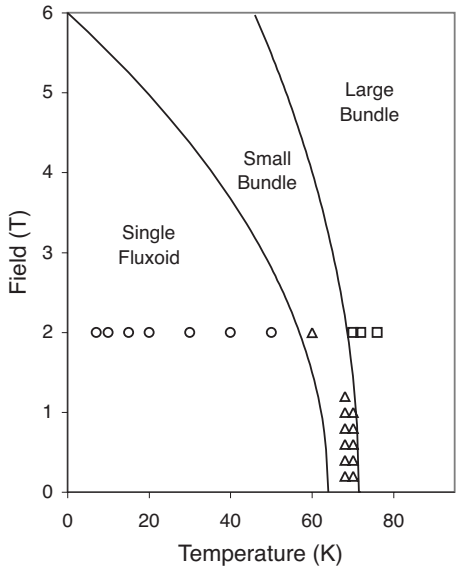

FIG. 5. Regions of hopping for flux flow in YBCO. Open circles are where the Webb length is equal to the maximum pinning model length, open triangles are where the Webb length is approximately three times the model length, and open squares are for where the Webb length is much greater than the model length.

two lengths agree can be interpreted as marking the region in phase space for single-fluxoid motion. When the lengths disagree, it can be interpreted as a sign of the transition to the small bundle regime. Note that there is no evidence for a phase change. We suggest that it is reasonable to interpret the near integer difference (a factor of 3) between the model length and the defined Webb length in the small bundle regime as the number of fluxoids in the small bundle. This finding also suggests that the basic physics of flux motion remains relatively unchanged in the transition to the small bundle regime.

Additional data taken at 2 T and at temperatures of 70 K and above show another large "jump" in the defined Webb length. This large increase in the four volume is an indication of the transition into the large bundle regime. It is now possible to use these measurements to delineate the phase diagram for correlated flux motion, as shown in Fig. 5. The solid lines are pinning regime boundaries that we take to be proportional to $(T_x - T)^{1/2}$, where T_x is the zero-field temperature boundary for small or large bundles. The temperatures are $T_{sb}=64$ K for small bundles and $T_{lb}=72$ K for large bundles. The zero-temperature field boundaries are taken from Blatter *et al.*[10] who calculate that $B_{sb}=6$ T for small bundles and $B_{lb}=10$ T for large bundles. This rather crude mapping of the phase space is nonetheless quite interesting and provides a useful guide to future investigations of fluxoid dynamics.

V. FLUXOID DAMPING AND MASS—RESULTS AND DISCUSSION

From the Bean model, a drop in the critical current represents a flow of magnetic flux toward the sample center, and treating our sample as a thin disk,[34] we estimate

$$dj/dt \approx 6B\bar{v}/\mu_0 rd, \tag{18}$$

where $\bar{v}$ is the average flux velocity, r is the effective sample radius, and d is the sample thickness. The average flux velocity can also be written as $\bar{v}=2\xi f_a \exp[-E_B/kT]$, where the mean jump distance is assumed to be 2ξ and f_a is the attempt frequency. Substituting this expression for $\bar{v}$ into Eq. (18) and comparing to Eq. (1), the rate equation, gives the prefactor as

$$K = 12B\xi f_a/\mu_0 rd. \tag{19}$$

The prefactor can be obtained from creep data using the measured barrier height $E_B(j_0)=(23.0\pm 0.5)kT$. At 10 K and 2 T, the prefactor is $K=3.5\times 10^{16}$ A/m^2-s giving $f_a=8.5\times 10^{10}$ Hz. It is interesting to compare this number with an estimate by Fischer, Fisher, and Huse[15] of the relaxation frequency of a zone boundary flux lattice "phonon"

$$\omega_{ZB} \cong 6\times 10^{10}\ \mathrm{s}^{-1}\left(\frac{H}{H_{C2}}\right)\left(\frac{\rho_n}{\mu\Omega\ \mathrm{cm}}\right)\left(\frac{100\ \mathrm{nm}}{\lambda}\right)^2,$$

where H_{C2} is the upper critical field and ρ_n is the normal state resistivity. Using $\rho_n=100\ \mu\Omega$ cm from Wuyts *et al.*[35] gives $\omega_{ZB}\cong 4\times 10^{10}$ s^{-1}. This order of magnitude agreement

between the measured attempt frequency and the calculated relaxation frequency is gratifying. Their observation that this "phonon" is overdamped supports the view presented in Sec. III that the fluxoid is able to sample its environment as it moves.

A rough estimate for the fluxoid mass can be obtained from the measured prefactor. Neglecting the drag and assuming a harmonic restoring force with stiffness constant $\kappa = 2E_B/\xi^2$ gives a mass for a segment 210 nm in length of

$$m = 2E_B/(2\pi\xi f_a)^2 \approx 10^{-26}\ \text{kg} \approx 10^4 m_e, \qquad (20)$$

where m_e is the free electron mass.

The mass of a fluxoid was first considered by Suhl.[36] A plausible interpretation of his analysis as applied to unconventional (high-temperature) superconductors[37] suggests a mass of one quasiparticle per conducting plane. The mean separation of conducting planes in YBCO is about 0.6 nm, thus the effective quasiparticle mass that would yield our above result is $m^* \approx 30 m_e$ or alternatively, $\ln[m^*/m_e] = 3.4 \pm 1$. This effective mass is plausible, particularly since the quasiparticles will involve Cu $3d$ orbitals. On the other hand, a number of additional contributions to fluxoid mass have been conjectured, but not considered here.[38]

VI. SUMMARY AND CONCLUSIONS

This work presents an extension of an alternative model of collective pinning (the maximum pinning model) to wider regions of the B,T phase space for superconducting YBCO. We began with a discussion of samples and preparation techniques and provided quantitative criteria for identifying samples that are collectively pinned (Sec. II). Avoiding the effects of strong pinning defects is crucial in studies of collective pinning. We close with some evidence that the superconducting fluxoid in YBCO is purely conventional (Sec. V). In-between (Secs. III and IV) we confront data and model predictions in three regimes. (A) At low temperature the simple maximum pinning model predicts $E_B \propto 1/j^\mu$ with $\mu = 1$ and $j(T) \propto 1/T$ in reasonable agreement with data in the literature. We show that the simple model predicts that the critical pinning length $l_{\max} \propto T^2$. This prediction is also in good agreement with low-temperature measurements of the four volume. (B) In the extended maximum pinning model we identify two contributions to the barrier height E_B: one due to direct near neighbor fluxoid-fluxoid interaction and a second that arises from the dynamics of the motion of fluxoid segments. These contributions to the barrier height can be written in terms of an artificial effective current density ∂j. This change accounts for $\mu \neq 1$, provides an improved fit to creep data, and predicts that $\mu(T) = 1 + cT$ as confirmed by data. Further the barrier height dependence on current density is modified from $E_B(j) \propto 1/j^\mu$ to $E_B(j) \propto 1/(j + \partial j)$. In agreement with the simple model, the new form of the barrier height also predicts that $l_{\max} \propto T^2$ except for the temperature dependence of material parameters and the effects of fluxoid thermal vibrations. (C) Plausible sources of $\partial j = j_r + j_s$ are presented in simple physical terms that allow the extension of the maximum pinning model to higher temperatures. The model provides agreement with experiment for $j(B,T)$ and $\mu(B,T)$ that sheds light on an interesting peak effect that is seen at relatively low temperature in samples dominated by collective pinning. As noted earlier, thermal averaging due to the vibration of single fluxoids reduces the effectiveness of point defect pinning. From Eq. (11), the vibration amplitude of a fluxoid is reduced by an increasing B until the effect saturates at large B. This effect will give rise to an increase in j with increasing B at low fields as the application of applied field increases the effectiveness of point defect pinning. At high field, j will fall with B simply because of the near neighbor repulsion between fluxoids (the lagging fluxoid segments are pushed off of their pinning sites). Ultimately, this same fluxoid-fluxoid interaction will lead to the coordinated hopping of bundles. From this point of view, the low-temperature peak effect in the single-fluxoid regime is simply a precursor to bundle motion on a larger scale. Combined with experimental four-volume measurements, this model provides for a determination of the phase regimes for single-fluxoid, small bundle, and large bundle fluxoid motion in collectively pinned YBCO.

Our conclusions are (1) the low-temperature regime is strictly single fluxoid, (2) the extended maximum pinning model provides an excellent description of $j(B,T)$ and the associated flux creep of single-fluxoid motion even up to 50 K, and (3) the measurement of the four volume provides a powerful investigative tool in the single-fluxoid regime.

The maximum pinning model provides a direct physical picture of the collective pinning of single fluxoids and provides a basis of understanding of pinning to build upon for the investigation of other phenomena of significant technological interest, including maximizing currents through collective pinning or a combination of collective and strong pinning defects.

*Also at Oak Ridge Associated Universities.

[1] J. G. Bednorz and K. A. Müller, Z. Phys. B: Condens. Matter **64**, 189 (1986).

[2] M. K Wu, J. R. Ashburn, C. J. Torng, P. H. Hor, R. L. Meng, L. Gao, Z. J. Huang, Y. Q. Wang, and C. W. Chu, Phys. Rev. Lett. **58**, 908 (1987).

[3] P. A. Lee, N. Nagaosa, and X. G. Wen, Rev. Mod. Phys. **78**, 17 (2006); P. W. Anderson, P. A. Lee, M. Randeria, T. M. Rice, N. Trivedi, and F. C. Zhang, J. Phys.: Condens. Matter **16**, R755 (2004).

[4] D. J. Van Harlingen, Rev. Mod. Phys. **67**, 515 (1995).

[5] P. L. Gammel, D. J. Bishop, G. J. Dolan, J. R. Kwo, C. A. Murray, L. F. Schneemeyer, and J. V. Waszczak, Phys. Rev. Lett. **59**, 2592 (1987).

[6] L. Civale, A. D. Markwick, T. K. Worthington, M. A. Kirk, J. R. Thompson, L. Krusin-Elbaum, Y. Sun, J. R. Clem, and F.

Holtzberg, Phys. Rev. Lett. **67**, 648 (1991).
[7] A. Umezawa, G. W. Crabtree, J. Z. Liu, H. W. Weber, W. K. Kwok, L. H. Nunez, T. J. Moran, C. H. Sowers, and H. Claus, Phys. Rev. B **36**, 7151 (1987).
[8] K. Mcelroy, J. Lee, J. A. Slezak, D. H. Lee, H. Eisaki, S. Uchida, and J. C. Davis, Science **309**, 1048 (2005).
[9] A. I. Larkin and Yu. N. Ovchinnikov, J. Low Temp. Phys. **34**, 409 (1979).
[10] G. Blatter, M. V. Feigelman, V. B. Geshkenbein, A. I. Larkin, and V. M. Vinokur, Rev. Mod. Phys. **66**, 1125 (1994).
[11] Y. Yeshurun, A. P. Malozemoff, and A. Shaulov, Rev. Mod. Phys. **68**, 911 (1996).
[12] J. W. Farmer, X. Ding, D. L. Cowan, and D. C. Bradford, Phys. Rev. B **54**, 637 (1996).
[13] D. R. Nelson and H. S. Seung, Phys. Rev. B **39**, 9153 (1989).
[14] A. Houghton, R. A. Pelcovits, and A. Sudbo, Phys. Rev. B **40**, 6763 (1989).
[15] D. S. Fisher, M. P. A. Fisher, and D. A. Huse, Phys. Rev. B **43**, 130 (1991).
[16] G. W. Crabtree and D. R. Nelson, Phys. Today **50**, 38 (1997).
[17] V. B. Geshkenbein and A. I. Larkin, Sov. Phys. JETP **68**, 639 (1989).
[18] H. Kupfer, T. Wolf, C. Lessing, A. A. Zhukov, X. Lancon, R. Meier-Hirmer, W. Schauer, and H. Wuhl, Phys. Rev. B **58**, 2886 (1998).
[19] J. R. Thompson, Yang Ren Sun, and F. Holtzberg, Phys. Rev. B **44**, 458 (1991).
[20] L. F. Schneemeyer, Nature (London) **329**, 423 (1987).
[21] Ruixing Liang, P. Dosanjh, D. A. Bonn, D. J. Baar, J. F. Carolan, and W. N. Hardy, Physica C **195**, 1992 (1992).
[22] M. R. Beasley, R. Labusch, and W. W. Webb, Phys. Rev. **181**, 682 (1969).
[23] J. W. Farmer, M. Kornecki, and D. L. Cowan, Int. J. Mod. Phys. B **12**, 3267 (1998).
[24] Y. Abulafia, A. Shaulov, Y. Wolfus *et al.*, Phys. Rev. Lett. **77**, 1596 (1996).
[25] Charles P. Bean, Rev. Mod. Phys. **36**, 31 (1964).
[26] Y. Abulafia, A. Shaulov, Y. Wolfus, R. Prozorov, L. Burlachkov, Y. Yeshurun, D. Majer, E. Zeldov, and V. M. Vinokur, Phys. Rev. Lett. **75**, 2404 (1995).
[27] M. P. Maley, J. O. Willis, H. Lessure, and M. E. McHenry, Phys. Rev. B **42**, 2639 (1990).
[28] M. V. Feigel'man, V. B. Geshkenbein, A. I. Larkin, and V. M. Vinokur, Phys. Rev. Lett. **63**, 2303 (1989).
[29] P. G. De Gennes and J. Matricon, Rev. Mod. Phys. **36**, 45 (1964).
[30] Charles P. Poole, Horacio A. Farach, and Richard J. Creswick, *Superconductivity* (Academic Press, San Diego, 1995).
[31] J. E. Sonier, R. F. Kiefl, J. H. Brewer *et al.*, Phys. Rev. Lett. **72**, 744 (1994); J. E. Sonier, J. H. Brewer, R. F. Kiefl *et al.*, Phys. Rev. Lett. **79**, 2875 (1997).
[32] E. H. Brandt, Phys. Rev. Lett. **63**, 1106 (1989).
[33] J. E. Sonier, J. H. Brewer, R. F. Kiefl, G. D. Morris, R. I. Miller, D. A. Bonn, J. Chakhalian, R. H. Heffner, W. N. Hardy, and R. Liang, Phys. Rev. Lett. **83**, 4156 (1999); J. E. Sonier, R. F. Kiefl, J. H. Brewer, D. A. Bonn, S. R. Dunsiger, W. N. Hardy, R. Liang, R. I. Miller, D. R. Noakes, and C. E. Stronach, Phys. Rev. B **59**, R729 (1999).
[34] M. Daumling and D. C. Larbalestier, Phys. Rev. B **40**, 9350 (1989).
[35] B. Wuyts, V. V. Moshchalkov, and Y. Bruynseraede, Phys. Rev. B **53**, 9418 (1996).
[36] H. Suhl, Phys. Rev. Lett. **14**, 226 (1965).
[37] N. B. Kopnin, in *Solid-State Sciences*, edited by R. P. Huebener, N. Schopohl, and G. E. Volovik (Springer, New York, 2002), Vol. 132, p. 113.
[38] *Solid State Sciences*, edited by R. P. Huebener, N. Schopohl, and G. E. Volovik (Springer, New York, 2002), Vol. 132.